Title

Experimental study on dynamical blocking conditions of net exchange flows

Permalink

https://escholarship.org/uc/item/48s7m6h9

Journal

International Symposium on Stratified Flows, 8(1)

Authors

Laanearu, Janek

Cuthbertson, Alan

Carr, Magda

et al.

Publication Date

2016-08-29

Experimental study on dynamical blocking conditions of net exchange flows

Janek Laanearu (1), Alan Cuthbertson (2), Magda Carr (3), Joel Sommeria (4), Madis-Jaak Lilover (5), Samuel Viboud (4) and Jarle Berntsen (6)

(1) Department of Mechanics, Tallinn University of Technology, Tallinn, Estonia, e-mail: janek.laanearu@ttu.ee
(2) School of Energy, Geosciences, Infrastructure and Society, Heriot Watt University, Edinburgh, UK, e-mail: a.cuthbertson@hw.ac.uk
(3) School of Mathematics, University of St Andrews, St Andrews, UK, e-mail: magda@mcs.st.uk
(4) Laboratoire des Ecoulements Géophysiques et Industriels, Grenoble, France, email: joel.sommeria@legi.grenoble-inp.fr
(5) Institute of Marine Systems, Tallinn University of Technology, Tallinn, Estonia, email: madis-jaak.lilover@msi.ttu.sea.ee
(6) Department of Mathematics, University of Bergen, Bergen, Norway, email: jarleb@math.uib.no.ac.uk

Abstract

Preliminary analysis of a series of large-scale experiments investigating bi-directional stratified flows across a submerged trapezoidal sill obstruction is presented. A range of parametric forcing conditions: i) variable fresh- and saltwater flow rates; ii) density differences; and iii) sill submergence depths are used to generate net-barotropic exchange flows. Detailed synoptic velocity fields are measured across the sill crest using PIV, while high-resolution density profiles are obtained using micro-conductivity probes sited at several channel and sill locations. These measurements are used to determine a relationship between the locations of i) the density excess 0.5-isopycnal interface, separating the intruding saline water from the overlying freshwater layer, and ii) the zero-velocity interface, defined by the reversal point of velocity profiles. Blockage of saline intrusions by strongly barotropic flows in the upper freshwater layer is detected under specific parametric combinations of the upper layer specific flow rate (Q_1/w_0), the reduced gravity (g') and the sill submergence depth (h_b).

1   Introduction

Within estuaries and tidal inlets, salt water near the bed can intrude upstream in the opposite direction to superimposed, upper-layer freshwater flows originating from river discharges and flowing towards the sea (Laanearu *et al*., 2011). Some estuaries can be completely blocked from marine water intrusions into the river basin, while others are strongly influenced by saline water circulations in the estuary mouth. The estuarine stratified flows can lead to significant depthwise variations and strong gradients in both velocity and density (see Laanearu *et al*., 2014). Sargent and Jirka (1988) have shown experimentally that the dynamics of arrested saline intrusions into estuaries can be represented by the position of two interfaces, namely i) the density interface, separating the intruding saline water from the outflowing fresh water layer and ii) the velocity interface, determined by a flow reversal point in the velocity profile. The interplay between the velocity and density fields of stratified flows under steady state conditions is determined by the force balance, where buoyant pressure gradients, shear stresses and convective accelerations dominate. However, the turbulent fluxes can result in significant

interfacial mixing and transfer of mass and momentum between the layers. In some cases, strong vertical entrainment is present within the region of the salt-water return flow, while, in other circumstances, interfacial waves are first formed at the density interface; the breaking of such internal waves providing an additional mechanism for vertical mixing across the density interface. Improved knowledge of the bottom boundary dynamics associated with the intrusion of marine waters into river basin is required to parameterise boundary layer processes associated with restricted, exchange flows across topographic obstructions. These processes are known to be crucial for water circulation, mixing, stratification, deep-water renewal, bottom stagnation and flushing within the semi-enclosed water bodies, such as fjords and estuaries.
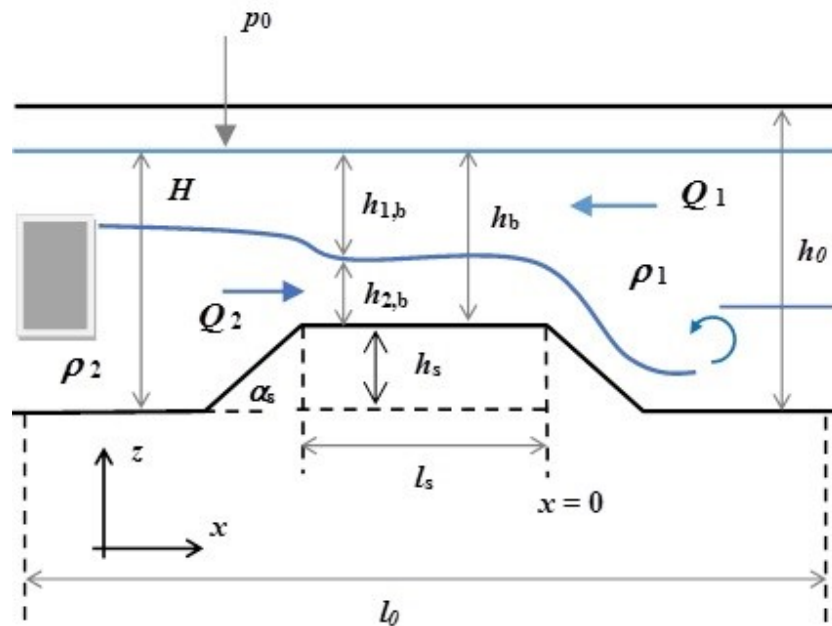

Figure 1: Schematic of the submerged trapezoidal sill obstruction and notations.

Internal hydraulic theory has been particularly useful in interpreting the stratified flow dynamics in straits and estuaries (Armi and Farmer, 1986; Dalziel, 1991; Laanearu and Davies, 2007). Zhu and Lawrence (2000) extended the internal flow model by including frictional and non-hydrostatic effects for the maximal exchange over a sill in a channel connecting two reservoirs of slightly different density. Cuthbertson *et al*. (2006) applied a similar two-layer exchange flow model for sub-maximal exchange to consider the case of a slowly descending barrier. In the recent study by Cuthbertson *et al*. (2016), the two-layer, bi-directional stratified flow model for rectangular-shaped channel have been extended to include both frictional and entrainment effects, which are required to account for turbulent stresses and mass loss in lower saline layer. In validating the internal flow hydraulic models, the experimental findings are useful in defining the parametric influences due to flow variations, density differences, water levels and channel shapes. The physical mechanisms associated with the arrested saline intrusions are, as yet, poorly investigated and therefore more experimental studies are needed.

The experimental program, funded under the EU FP7 Hydralab IV Initiative, is conducted in a large-scale facility (Coriolis Platform II) at Laboratoire des Écoulements Géophysiques et Industriels (LEGI), Grenoble (France). A trapezoidal-shaped, impermeable sill obstruction is used to generate net-barotropic exchange flows (see schematic in Figure 1). Measurements focused on obtaining velocity and density fields under a range of parametric

forcing conditions: i) variable fresh- and saltwater flow rates, ii) density differences and iii) water levels. Detailed synoptic velocity fields are analysed across the sill obstruction using 2D Particle Image Velocimetry (PIV), with high-resolution density profiles obtained using micro-conductivity probes. These experimental measurements are processed to define parametric conditions under which the saline intrusions become arrested through interfacial mixing at the intrusion nose by the upper, counter-flowing, freshwater layer. Experimental results are also intended to give higher Reynolds numbers that are more representative of real situations. In exchange flow problems with net-barotropic component in surface layer, the internal flow dynamics are expected to be sensitive to i) the dimensions of the obstruction (i.e. sill length, height and submergence depth), ii) density differences (i.e. stratification) between the two water bodies separated by the sill obstruction and iii) external forcing conditions due to tidal and freshwater inflows. In this context, however, the range of parametric conditions under which these restricted exchange flows are initiated (or indeed blocked), are not well understood. In addition, further research is required to investigate the physical mechanisms associated with shear-induced mixing processes, vertical entrainment and the generation of interfacial waves by bi-directional stratified flows across the sill obstructions.

2   Experiments

2.1   Facility

A rectangular flume of length $l_0 = 9$ m, width $w_0 = 1.5$ m and depth $h_0 = 1.2$ m is used to generate flows across a submerged trapezoidal sill obstruction (Figure 1 and 2). The flume is constructed within the circular basin of 13 m-diameter and 1.2 m-deep, allowing total water depths H of up to 1.0 m. The rectangular channel incorporates a rigid trapezoidal obstruction with a horizontal sill length $l_s = 2$ m, sill crest height $h_s = 0.5$ m above the channel floor, and inclined approaches to the sill crest set at an angle $\alpha_s = 26.57°$ on both sides. The walls of the central 6 m-long section of the channel, along with the sill obstruction itself, are constructed from transparent Plexiglas to facilitate flow illumination by laser (Figure 2).

2.2   Set up

The counter-flowing layers of saline water ($\rho_2 = 1004.7 - 1009.6$ kg.m^{-3}) and overlying freshwater ($\rho_1 = 1000 - 1001.1$ kg.m^{-3}) are driven across the submerged sill obstruction. The saltwater is directed into the channel via a gravity feed system, and is injected directly into the bottom of the marine basin **M** through a 0.3 m-high by 1.5 m-wide rectangular manifold section. The fresh ambient water is recirculated within the channel and the surrounding circular tank by two centrifugal pumps located in the upper part of basin **M**, directly above the saline water manifold. These two injection systems provided fresh- and saltwater volume fluxes in the range $Q_1 = 0 - 30$ l.s^{-1} and $Q_2 = 2.64 - 6.94$ l.s^{-1}, respectively. With the circular basin filled to a total depth $H = 0.85 - 0.95$ m, the saline water volume flux is carefully fed into the bottom of the basin **M** to avoid excessive initial mixing with the overlying ambient freshwater part. Once the saline water layer thickness approached the sill crest elevation (i.e. $h_s = 0.5$ m), the gravity-driven feed of saltwater is increased to the desired volume flux Q_2. At this point, a dense saline water overflow layer develops across the sill spilling into the impoundment (river) basin **I**, which after a short period of time reaches a quasi-steady spill condition for the initial $Q_1 = 0$ case (i.e. with no counter-flowing freshwater flow). During the subsequent run, the counter-flowing freshwater volume flux is increased incrementally (i.e. $Q_1 = 0 \rightarrow 3 \rightarrow 8 \rightarrow 12 \rightarrow 21$

$\rightarrow$ 26 $\rightarrow$ 30 l.s^{-1}) at prescribed elapsed times t. Thus, the parametric dependence of the net exchange flow conditions developed across the sill obstruction is tested in relation to i) the relative submergence depth of the sill, i.e. $h_b/H = 1 - h_s/H = 0.41$ - 0.47; ii) the relative density difference of the fresh- and saltwater inflows, i.e. $(\rho_2 - \rho_1)/\rho_1 = 0.005$ - 0.01; and iii) the ratio of fresh and salt water volume fluxes, i.e. $q^* = Q_1/Q_2 = 0$ - 11.36.

3.2   Instrumentation

Experimental measurements focused mainly on obtaining high temporal and spatial resolution density and velocity fields both across the sill obstruction and at selected locations within basins **M** and **I** (see Figure 2). Flow illumination is provided by a continuous laser system sited at the far end of basin **I**, which produced a vertical laser light sheet aligned along the channel centreline. Two-dimensional PIV is then used to measure velocity fields within the resulting vertical (xz) plane (see Figure 1), employing two side-mounted digital CCD cameras to record both instantaneous and synoptic (i.e. time-averaged) flow velocity fields within specific regions of interest (i.e. across the 2 m-long sill section and on the down-sloping face of the sill obstruction into basin **I**). Post-processing of these velocity field measurements is conducted using in-house PIV software (UVMAT).

High-resolution density profile measurements are also obtained at key locations both across the sill obstruction and within basin **M** using an array of motorized micro-conductivity probes (Head, 1983), while a 3D Acoustic Doppler Velocimeter (ADV) probe is utilized to measure detailed velocity profiles at a similar measurement location to a micro-conductivity probe, in order to gain insight on vertical gradients of velocity-density profiles for the restricted exchange flows generated under different parametric conditions outlined above. These micro-conductivity probes (and the ADV probe) traversed vertically through the full depth of the developed stratified flows at a rate of descent of 5 mm.s^{-1}. (Note: ADV velocity measurements are essentially used to calibrate the source fresh water volumetric fluxes in the channel under a range of different centrifugal pumping motor speeds). More detailed description of the measurement procedure in the LEGI experiments is presented in Cuthbertson *et al.* (2016).
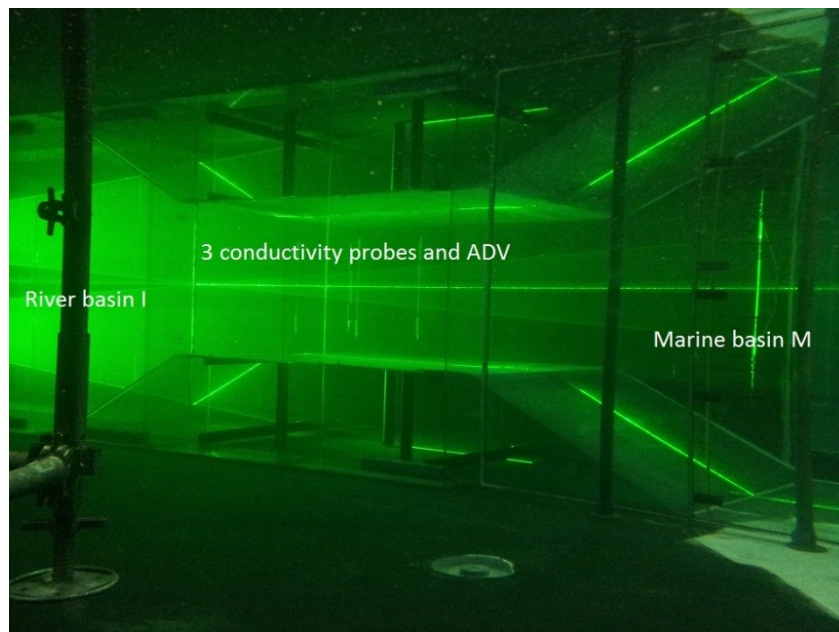

Figure 2: A side image of the submerged trapezoidal sill obstruction. The conductivity probes and ADV at the sill crest, between basins **I** and **M**, are visible in the image.

3   Preliminary analysis

3.1   Internal flow structure

Inspection of the synoptic velocity fields across the sill crest, and corresponding density profiles, measured at several sill locations, reveals the internal-flow structure of the bi-directional stratified flows generated in the experimental runs under investigation. These restricted exchange flows can be characterized by two interfaces: i) the elevation of the density-excess $\rho' = (\rho(z) - \rho_2)/(\rho_1 - \rho_2) = 0.5$ isopycnal, obtained from vertical sorting of the measured density profiles, separating the intruding saline water from the overlying freshwater flow; and ii) the zero-velocity interface elevation, determined by a flow reversal point in the velocity profiles obtained from PIV measurements. In this way, a non-dimensional density interface height $(h_{2,b} + h_s)_{density}/H$ can be plotted versus the corresponding non-dimensional velocity interface height $(h_{2,b} + h_s)_{velocity}/H$ at the sill crest location $x/l_s = -0.5$ for the runs (i) - (vii) of the experiments EX2 - EX7 (Figure 3).
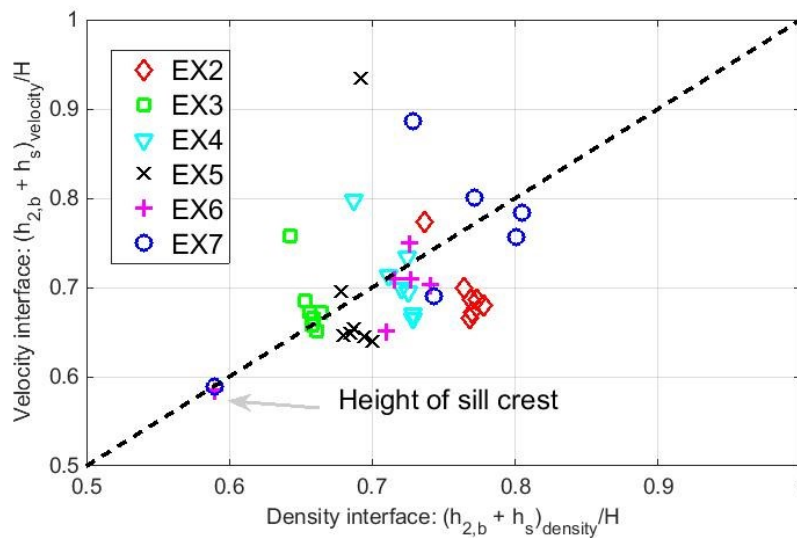

Figure 3: A non-dimensional density excess $\rho' = 0.5$ isopycnal height versus a non-dimensional zero-velocity interface height at the sill crest location $x/l_s = -0.5$ for the runs (i) - (vii) of the experiments EX2 - EX7.

It should be noted that both the velocity and density profiles include uncertainties due to turbulent fluctuations, interfacial wave activities, and some experimental measurement errors. However, the results presented in Figure 3 show that the zero-velocity interface is slightly lower than the density excess interface. According to findings from "salt-wedge" type experimental studies (e.g. Sargent and Jirka, 1988; Laanearu *et al.*, 2014), the velocity and density interfaces are vertically diverged far from the fresh-water source. However, direct comparisons of measured density and velocity interfaces heights in the current study reveals that the divergence of the zero-velocity and density excess 0.5-isopycnal interfaces is comparatively small. This is expected in the vicinity of the fresh-water source (i.e. at $x/l_s > -0.5$) for cases with net-barotropic component in the surface layer. The increased interfacial shear instability due to stronger local net-barotropic flow conditions (i.e. $q \gg 1$) results with entrainment and mixing of dense saline water into the overlying, outflowing freshwater layer. These experimental findings are designed to aid qualitative and quantitative interpretation of the internal-flow processes associated with the lower saline intrusion layer blockage conditions,

and indicate that the primary mechanism for this blockage is mass loss from the saline intrusion layer due to significant interfacial mixing and entrainment (Cuthbertson *et al.*, 2016).

3.2 Saline intrusion blockage

In experimental runs, the development of bi-directional stratified flows across the sill obstruction are measured for both net lower layer ($q^* < 1$) and upper layer ($q^* > 1$) barotropic flow components. Experimental parameters for runs EX2 - EX7 are presented in Table 1. Within the majority of experiments (EX2 - EX5), the upper freshwater flow is insufficient to completely arrest the saline intrusion across the trapezoidal sill obstruction. However, the overlying freshwater flow is able to block the saltwater intrusion at the sill crest in the two experiments EX6 and EX7, and this at different values of the parameter $q^* > 1$. The key difference between fixed parametric conditions in experiments EX6 and EX7 is the saltwater flow rate: $Q_2 = 2.92$ l.s^{-1} and 6.94 l.s^{-1}, respectively, with other parametric conditions remaining largely unchanged (i.e. sill submergence depth $h_b \approx 0.35$ m and reduced gravity $g' = 0.046$ m.s^{-2}). A complete blockage of the saline intrusion only occurs in runs (vi)-(vii) of EX6 and EX7, where the freshwater flow rate $Q_1 > 21.0$ l.s^{-1}.

Table 1: Experimental parameters for the runs (i) - (vii) of the experiments EX2 - EX7.

Exp.	ρ_1 (kg.m^{-3})	ρ_2 (kg.m^{-3})	g' (m.s^{-2})	Q_1 (l.s^{-1})	Q_2 (l.s^{-1})	h_b (m)	H (m)
EX2	1000.0	1005.1	0.050	0.0-30.0	6.94	0.430	0.930
EX3	1000.0	1009.6	0.094	0.0-30.0	6.94	0.450	0.950
EX4	1000.0	1009.6	0.094	0.0-30.0	6.94	0.350	0.850
EX5	1000.0	1009.6	0.094	0.0-30.0	2.64	0.350	0.850
EX6	1000.0	1004.7	0.046	0.0-30.0	2.92	0.354	0.854
EX7	1000.0	1004.7	0.046	0.0-30.0	6.94	0.349	0.849

A non-dimensional source freshwater volume flux $Q_1^2/(g'w_0^2h_b^3)$ is plotted versus the ratio of fresh- and saltwater flow rates $q^* = Q_1/Q_2$ for the runs (i) - (vii) in experiments EX2 - EX7 as shown in Figure 4. This figure is assembled for the fixed parametric conditions (Q_2, g', h_b) under which the experimental runs are performed for varying exchange flow net-barotropic component in the surface layer (i.e. Q_1). The magnitude of normalised freshwater flux also indicates the parametric conditions under which full saline blockage occurs, with a critical value of $Q_1^2/(g'w_0^2h_b^3) \sim 0.125$ required for blockage (i.e. irrespective of the fresh- and saltwater flow ratio $q^* = Q_1/Q_2$). Within the majority of experiments the water level is relatively high, i.e. $H \sim 0.94$ m (EX2 - EX3), or/and the stratification is relatively strong, i.e. the reduced gravity is large $g' = 0.094$ m.s^{-2} (EX3 - EX5), and therefore the upper freshwater flow is apparently insufficient to completely block the saline intrusion across the sill crest (cf. Table 1). The results presented in Figure 4 also indicate the freshwater flow rate Q_1 under which the full saline blockage may occur in the experiments EX2 - EX5. It is interesting to note that the net-barotropic exchange flows generated across the sill crest become arrested under different q^* values, and this to maintain a critical value of the non-dimensional source freshwater volume flux $Q_1^2/(g'w_0^2h_b^3)$. Thus net-barotropic exchange flows are suggesting that full saline blockage across at the sill obstruction occurs when the submergence depth h_b and reduced gravity g' are both reduced under the range of q^* tested.
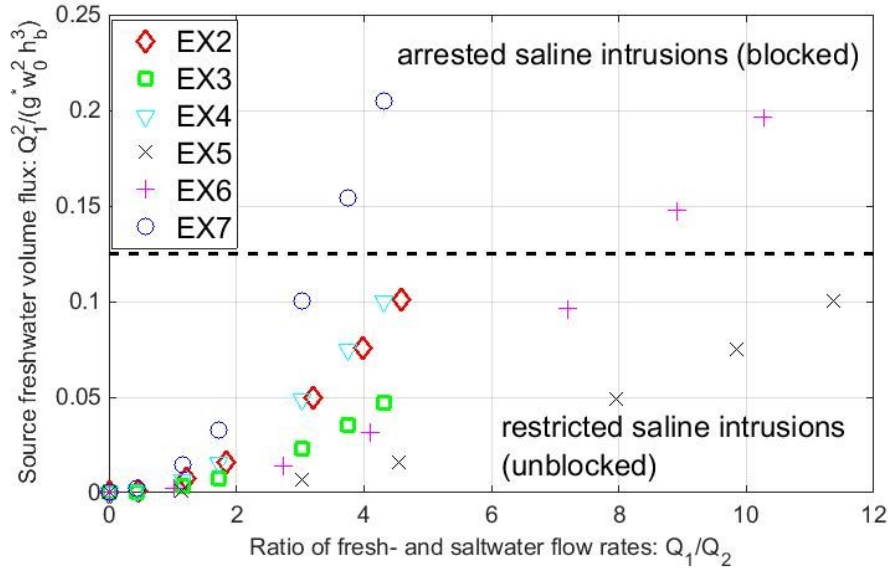
Figure 4: The non-dimensional source freshwater volume flux versus the fresh- and saltwater flow rates ratio (q^*) for runs (i) - (vii) of the experiments EX2 - EX7.

4   Concluding remarks

The observed internal-flow structure shows that the turbulent fluxes within the strong interfacial shear layers result in significant interfacial mixing and transfer of mass and momentum between the fresh- and saltwater layers. The velocity and density measurements along the sill crest confirm that the divergence of the zero-velocity ($u = 0$) and density excess ($\rho' = 0.5$) interfaces is comparatively small in the vicinity of fresh-water source (i.e. at $x/l_s > -0.5$) for the net-barotropic exchange flows investigated. The experiments confirm that in some runs the submerged trapezoidal sill can completely block the saltwater intrusion into basin **I**, and in other runs the strong influence of saline water circulations is present, with restricted intrusion of saline water into basin **I**, flowing in the opposite direction with the overlying layer of turbulent freshwater flow. The experimental findings show that the bi-directional stratified flows generated across the trapezoidal sill crest become arrested under different fresh- and saltwater flow ratio (Q_1/Q_2) values, and this to maintain a critical value of the non-dimensional source freshwater volume flux $Q_1^2/(g'w_0^2 h_b^3)$. Surprisingly, the parametric importance of trapezoidal sill height (h_b) on dynamical blocking conditions of net exchange flows with the barotropic component in surface layer is not pronounced. Further research is required to investigate the physical mechanisms associated with shear-induced mixing processes, vertical entrainment and the generation of interfacial waves in the stratified flows at topographic obstructions.

As a next step, the internal-flow hydraulic theory can be used for interpretation of observed dynamics of restricted exchange flows across the sill obstruction. In this regard, the internal-flow hydraulic models can be modified for the cases of net-barotropic exchange flows (as in Cuthbertson *et al.* 2016). In Zhu and Lawrence (2000) two control-point model the interface elevations of the zero-net exchange, measured at different sections, both in the vicinity of the sill obstruction and at more remote channel locations, corresponded well to the theoretically predicted elevations when the internal flow head loss was specified in the range 0.0 − 0.1 of the total fluid depth. However, in the case of restricted exchange, the internal-flow hydraulic regime across the sill obstruction can be only sub-critical. The two-layer, bi-directional flow hydraulic models for rectangular-shaped channel can be simply extended to

include both frictional and entrainment effects, which are required to account for turbulent stresses and mass losses of lower saline layer. As such, the experimental results of the LEGI experiments can be used to validate two key parameters of the internal-flow hydraulic model, namely: i) the local flow rate ratio of upper fresh and lower saline layers; and ii) the mass loss in the lower saline layer. In this regard, it is anticipated that the theoretical findings will provide an important step towards achieving improved understanding of interfacial mixing and boundary layer processes within regions of restricted exchange (e.g. semi-enclosed estuaries and fjords), as well as providing new information for validation of numerical models.

5   Acknowledgements

6   References

Armi, L. and Farmer, D.M. (1986). Maximal Two-Layer Exchange through a Contraction with Barotropic Net Flow. *J. Fluid Mech.*, 164:27–51.

Cuthbertson, A. J. S., Laanearu, J., and Davies, P. A. (2006). Buoyancy-driven two-layer exchange flows across a slowly submerging barrier. *Environ. Fluid Mech.*, 6, 133–151.

Cuthbertson, A.J.S, Laanearu, J., Carr, M., Sommeria, J. and Viboud, S. (2016). Blockage of saline intrusions in restricted, two-layer exchange flows across a submerged sill obstruction. Submitted to the journal: *Environ. Fluid Mech*.

Dalziel, S. B. (1991). Two-layer hydraulics: a functional approach. *J. Fluid Mech.*, 223:135–163.

Head, M. J. (1983). The Use of Four Electrode Conductivity Probes for High Resolution Measurement of Turbulent Density or temperature Variation in Salt-Stratified Water Flows, Ph.D. Dissertation, University of California, San Diego, USA.

Laanearu, J. and Davies, P. A. (2007). Hydraulic control of two-layer flow in "quadratic"-type channels. *J. Hydraul. Res.*, 45(1): 3–12.

Laanearu, J., Vassiljev, A. and Davies, P. A. (2011). Hydraulic modelling of stratified bi-directional flow in a river mouth. *Proceedings of the Institution of Civil Engineers: Engineering and Computational Mechanics*, 164(4): 207–216.

Laanearu, J., Cuthbertson, A. J. S. and Davies, P. A. (2014). Dynamics of dense gravity currents and mixing in an up-sloping and converging vee-shaped channel. *J. Hydraul. Res.*, 52(1): 67–80.

Sargent, F. E. and Jirka, G. H. (1988). Experiments on Saline Wedge. *J. Hydraul. Eng. ASCE.*, 113(10): 1307–1323.

Zhu, D. Z. and Lawrence, D. A. (2000). Hydraulics of exchange flows. *J. Hydraul. Eng. ASCE.*, 126: 921–928.